PHYSICAL REVIEW D **91,** 083013 (2015)

Evidences of an innermost stable bound orbit predicted by general relativity from the amplitude of the twin-peak quasiperiodic oscillations

C. Germanà[*] and R. Casana

Departamento de Física, Universidade Federal do Maranhão, São Luís, MA, Brazil

(Received 30 July 2014; published 29 April 2015)

The twin-peak high-frequency quasiperiodic oscillations (HFQPOs), observed in the power spectra of low-mass x-ray binaries, might carry relevant clues about the physics laws reigning close to a compact object. Their frequencies are typical of the orbital motion time scales a few gravitational radii away from the compact object. The aim of the manuscript is to propose an intuitive model explaining that the energy carried by the lower high-frequency quasiperiodic oscillation can be related to differences of potential energy released by clumps of plasma spiraling in a curved space-time. Our model provides estimates on both the size of clumps of matter that can survive to the strong tidal force and energy loaded by tides on the clump. We also have obtained some constrains on the mechanical properties of the plasma orbiting into the accretion disk. We note that the systematic behavior of the emitted energy as a function of the central frequency of the lower HFQPO, observed in several sources with a neutron star, might give clues related to an innermost stable bound orbit predicted by the general relativity theory in strong field regime.

DOI: 10.1103/PhysRevD.91.083013 PACS numbers: 95.30.Sf, 91.60.Ba, 97.10.Gz, 97.80.Jp

I. INTRODUCTION

Since their discovery [1], the twin-peak high-frequency quasiperiodic oscillations (HFQPOs) observed in the power spectra of low-mass x-ray binaries (LMXBs) have attracted much attention. The HFQPOs have frequencies that correspond to the time scales of the orbital motion close to the compact object (milliseconds). They are believed to be produced by orbiting inhomogeneities of the density of the accretion disk, often referred as to clumps/blobs of matter [2–5], or to oscillation modes of the accretion disk [6–8]. Twin-peak HFQPOs might be potential probes to disclose the imprints produced by the orbiting matter in a strongly curved space-time, e.g., the signature of an innermost stable circular orbit (ISCO) predicted by general relativity (GR) in strong field [9,10], as well as the modulations of the x-ray flux by the precession of the orbits (see Refs. [11,12] for review). HFQPOs can also be used to constrain fundamental quantities of the compact object, such as its mass m and angular momentum a [13]. Attempts to estimate such quantities in systems with a neutron star (NS LMXBs) were done soon after the discovery of HFQPOs [14,15]. Most recently, Motta *et al.* [16,17] gave measurements of both m and a of black hole LMXBs. The observed frequencies of the HFQPOs were linked to the relativistic frequencies as in the relativistic precession model (Ref. [3]), where the upper peak in frequency of the twin-peak HFQPOs is linked to the Keplerian frequency ν_k of the orbiting matter, while the lower peak to the periastron precession frequency ν_p of the orbit. Different interpretations [15] and models linking ν_k to the lower HFQPO [18–20] were also proposed.

The unprecedented possibility of constraining the space-time around a compact object through HFQPOs and the idea of preferred orbital radii where HFQPOs would be produced have stimulated several works based on resonance mechanisms. Resonance between relativistic epicyclic and Keplerian frequency of the orbiting matter has been proposed to justify the observed $3:2$ ratio of the twin-peak HFQPOs [21–24]. Other resonance mechanisms propose forced oscillations in the accretion disk induced by the magnetic field of the neutron star [25], or resonance because of coupling between the oscillation modes of the orbiting matter in the disk and the spin of the neutron star [26–30]. Also, substantial work was done to test the models with the observed data and constrain both m and a of the compact object [31–33].

Besides being potential probes to study the motion of matter in a strongly curved space-time, works were devoted to illustrate other properties of the HFQPOs. de Avellar *et al.* [34] and Barret [35] reported time lags between photons from twin peaks as collected in different energy bands in NS LMXBs. Such lags were previously also noted in Ref. [36]. Thanks to the larger sample of collected data, de Avellar *et al.* [34] and Barret [35] were able to get finer results. This information may shine light on the emission mechanisms in such an extreme environment [37].

Barret *et al.* [38,39] and Méndez [40] analyzed the coherence Q of the twin peaks, defined as $Q = \nu/\Delta\nu$, where ν is the central frequency of the peak and $\Delta\nu$ its width. In several NS LMXBs, the Q-factor of the lower HFQPO displays a steep increase and then an abrupt drop as a function of the central frequency ν of the peak. It was proposed that the abrupt drop of the Q-factor might be caused by the approach of the oscillation to ISCO [38], thus

[*]claudio.germana@gmail.com; claudio.germana@ufma.br

a geometry-related effect. However, this interpretation was debated in Refs. [40,41]. If confirmed, a signature of ISCO is of relevant importance, because it is predicted by GR in the strong field regime. In Refs. [38–40,42] is reported the amplitude of the twin-peak HFQPOs as a function of their central frequency. Like the quality factor Q, the behavior of the amplitude (the energy carried by the QPOs) of the lower HFQPO displays a systematic trend with an increase and then a slightly steeper decrease for increasing central frequency of the peak. The amount of energy released is up to ∼20% the total flux of the source in NS LMXBs ($10^{34} - 10^{36}$ erg/s, from atoll to Z sources [40]). But, how this huge quantity of energy is produced is not yet understood.

Matter orbiting close to a compact object experiences a strong tidal force. The effects of the encounter of stars with massive black holes were studied by a certain number of authors [43–47] and are of interest for the flaring activity observed at the center of galaxies [48]. Reis *et al.* [49] reported a QPO in the x-ray flux coming from the tidal disruption of a star by a supermassive black hole. Most recently, Del Santo *et al.* [50] linked to the tidal disruption of a planet by a white dwarf the x-ray flaring activity observed in the source IGR J17361-4441. Subsequent analysis revealed a QPO in the x-ray flux produced by such event [51].

The work done by tides is a significant source of energy already in our Solar System. The volcanism in Jupiter's moon Io is sustained by tides. Thus, it could be relevant to take into account the gravitational energy extracted through tides by the orbiting matter close to the compact object in LMXBs. Kostić *et al.* [52] modeled the signal from the tidal disruption of small satellites orbiting a Schwarzschild black hole. Germanà *et al.* [53] showed a simulated power spectrum with such code. For the first time a power spectrum alike to the observed ones in LMXBs is reported: both the power law and twin-peaks are reproduced.

The shape of the amplitude of the lower HFQPO, as a function of its central frequency (Fig. 1 in Ref. [42], Fig. 3 in Ref. [38], and Fig. 2 in Ref. [40]) is typical of the potential energy released by matter spiraling in a curved space-time. We believe that it might be worthwhile to investigate such an issue. In the following, we concentrate on the lower HFQPO. We show for the first time that the energy carried by the lower HFQPO can be accounted for by the gravitational energy extracted by spiraling clumps of matter undergoing the work done by the strong tidal force. We make use of the Schwarzschild potential as a first-order approach to the problem and check our calculations also in the Kerr metric. We show that the Schwarzschild/Kerr gravitational energy extracted over different regions of the space-time reproduces the observed bell-shaped behavior of the amplitude of the lower HFQPO [38–40,42]. The physical mechanism here proposed suggests that the behavior may be an effect related to an innermost marginally stable orbit predicted by GR in the strong field regime, below which no stable orbital motion can exist [9]. Because in theory such an orbit can have a generic eccentricity e [54], in a more general way we refer to it as the innermost stable bound orbit (ISBO) instead of ISCO.

The manuscript is organized as follows. In Sec. II we review the main features of the Schwarzschild potential and give new hints on a possible way to reveal a signature of ISBO. Section III and Sec. IV provide constrains on the maximum size allowed by tides of orbiting clumps of solid-state and plasma-state matter, respectively. In Sec. V we estimate both the energy loaded by tides per periastron passage on an orbiting clump of plasma and the amount of gravitational energy that would be emitted after tidal disruption of the clump. Section VI shows our results in the Kerr metric. In Sec. VII we comment on other factors that might affect a signature of ISBO and show (Sec. VII B) an interpretation accounting for the observed coherence of the lower HFQPO as a function of the luminosity of the source. Section VIII summarizes the conclusions.

II. SCHWARZSCHILD POTENTIAL SHAPE AND ISBO

We are interested in estimating differences of potential energy released by matter spiraling between the orbits in a curved space-time. For self-consistency, we review some of the well-known features of the gravitational potential in the Schwarzschild metric. Most importantly, we highlight new hints about a way of revealing a signature of ISBO.

The familiar radial effective Schwarzschild potential per unit mass μ of an orbiting particle reads [54]

$$V_{\text{eff}} = 1 - \frac{2m}{r} - \frac{2m\tilde{L}^2}{r^3} + \frac{\tilde{L}^2}{r^2} \tag{1}$$

where m is the mass of the compact object and $\tilde{L}$ is the angular momentum[1] of the particle (per unit mass μ) on the orbit of semilatus rectum p and eccentricity e

$$\tilde{L} = \left(\frac{p^2 m^2}{p - 3 - e^2}\right)^{1/2}. \tag{2}$$

The quantity p is defined such that the periastron of the orbit $r_p = pm/(1+e)$ and for bound stable orbits $p \geq 6 + 2e$ [54]. The second and third term in (1) refer to the gravitational potential in the Schwarzschild metric, while the forth term is the centrifugal potential. The attractive

[1]The quantities here reported are expressed in geometric units $G = c = 1$, unless differently specified. The mass m in geometric units is equal to the gravitational radius of the compact object $r_g = GM/c^2$, where M is the mass of the compact object in international system units, G the gravitational constant, and c the speed of light. For a $2M_\odot$ neutron star $r_g \sim 3$ km.

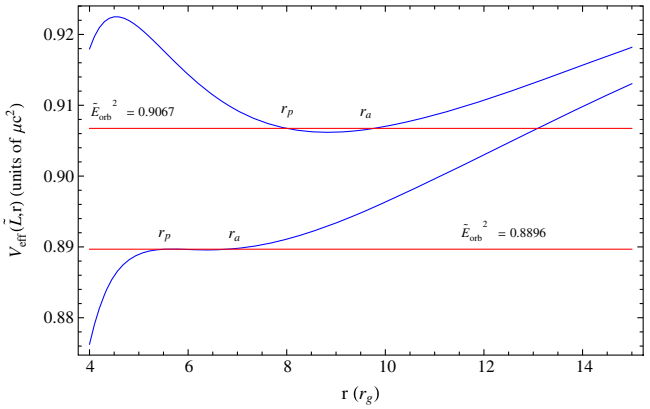

FIG. 1 (color online). Effective Schwarzschild potential as a function of the radial coordinate r for two different orbits of given specific angular momenta $\tilde{L}$ (blue curves). The periastra of the orbits are $r_p = 5.6r_g$ (ISBO) and $r_p = 8r_g$. The apastra are at $r_a = 6.8r_g$ and $r_a = 9.8r_g$, respectively. Red lines show the orbital energy $\tilde{E}^2_{\rm orb}$.

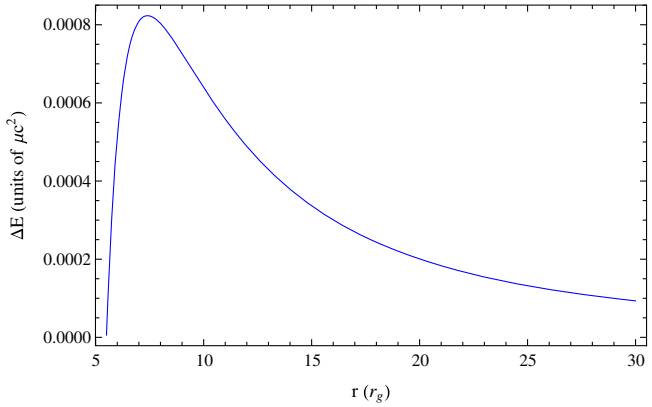

FIG. 2 (color online). Difference of potential energy at periastron between two orbits with periastra $0.1r_g$ away. The energy expected to be released draws a bell-like shape, decreasing towards ISBO ($r_p = 5.6r_g$) and displaying its maximum in the range of radii $r_p \sim 6.5 - 10r_g$.

term $\propto 1/r^3$ is relevant close to the compact object, i.e., when $r \sim r_g$ and causes the precession of elliptical orbits [55].

Figure 1 shows the known shape of the Schwarzschild potential for two different orbits. The blue lines draw the potential well for orbits of eccentricity $e = 0.1$ and periastra $r_p = 8r_g$ (top blue curve) and the ISBO $r_p = 5.6r_g$ (bottom blue curve).[2] The square of the orbital energy $\tilde{E}^2_{\rm orb}$ (in units of mass μ) is reported (red lines) and reads [54]

$$\tilde{E}^2_{\rm orb} = \frac{(p-2-2e)(p-2+2e)}{p(p-3-e^2)}. \tag{3}$$

The abscissas of the crossing points between $\tilde{E}^2_{\rm orb}$ and $V_{\rm eff}$ are the periastron r_p and the apastron r_a of the orbit and come from the solution of the equation $(dr/d\tau)^2 = \tilde{E}^2_{\rm orb} - V_{\rm eff} = 0$ [54]. The ISBO at $r_p = 5.6r_g$ has a less deep minimum than the orbit at $r_p = 8r_g$. It is because the term $\propto 1/r^3$ in (1) starts dominating.

The flattening of the minimum of the potential is a well-known feature of GR [56]. Besides the precession of the orbits that has already been measured in the case of Mercury (but in a weak field regime), the observational implications of the term $\propto 1/r^3$ in (1) in a strong field regime could be unmasked by the potential energy released by spiraling matter close the compact object. It is well known from the accretion theory [57] that if matter accretes from an orbit at $r = ar_g$ and ends up onto an inner orbit at $r = br_g$ ($b < a$), the energy released is the difference of potential energy between the two orbits. Such spiraling motion may be caused because of, e.g., the removal of orbital energy by tides acting on the clump of matter [58].

[2]For an orbit with $e = 0$ (ISCO), $r = 6r_g$.

Figure 2 shows a possible and simple way that could disclose a signature of ISBO. It depicts the behavior of the difference of the Schwarzschild potential, taken at periastron, between two orbits with periastra, e.g., $0.1r_g$ away. The orbits have a low eccentricity $e = 0.1$. The range of periastra is from $r_p = 30r_g$ to the ISBO at $r_p = 5.6r_g$. Such difference of potential energy between the two orbits, expected to be released, draws a bell-like shape: it increases up to $\sim 7.5r_g$ and then decreases up to ISBO. This characteristic shape is a consequence of the term $\propto 1/r^3$ in (1). In a Newtonian potential the differences of potential keep increasing in absolute value towards the inner regions. Thus, an observational evidence of the term $\propto 1/r^3$ in (1), and therefore of ISBO, might be through these energetic considerations. We stress that these arguments have not yet been highlighted in the literature.

In Refs. [38,40,42] it is shown that the energy (the amplitude) carried by the lower HFQPO in NS LMXBs, as a function of its central frequency, draws a bell-shaped behavior like that around the maximum of Fig. 2. The central frequency of the lower HFQPO is typical of the orbital motion within $r \sim 6.5 - 10r_g$. It may be worthwhile to investigate whether the observed behavior originates from differences of potential energy released by spiraling matter.

III. SIZE ALLOWED BY THE STRONG TIDES OF ORBITING CLUMPS OF MATTER: THE SOLID-STATE CASE

The arguments in Sec. II give general clues about the overall pattern of the potential energy (in units of rest-mass energy) released by spiraling matter between orbits $0.1r_g$ away over different regions of the space-time, to compare it to the observed pattern reported in Fig. 1 in Ref. [42], Fig. 3 in Ref. [38], and Fig. 2 in Ref. [40]. We investigate whether

this mechanism could actually account for the observed energy carried by the lower HFQPO ($10^{34}-10^{36}$ erg/s, from atoll to Z sources [40]). We need to give an estimate on the mass of the clumps of matter. The strong tidal force around a compact object sets an upper limit on their size.

Consider a spherical clump of matter of radius R and its cup of height $h = R/10$ at the distance $\sim R$ from the center of the clump. The volume of the cup is $V = \pi h^2(R - h/3)$, thus its mass is $\mu' = \rho V$, where ρ is the density of the material. The effective gravitational force acting on the cup at distance $r - R$ from the compact object is

$$F_{\rm eff} = \mu' c^2 \left(\frac{dV_{\rm eff}}{dr}\right)_{(r-R)} = \mu' c^2 \left(\frac{2m}{(r-R)^2} + \frac{6m\tilde{L}^2}{(r-R)^4} - \frac{2\tilde{L}^2}{(r-R)^3}\right) \quad (4)$$

where $V_{\rm eff}$ is from (1) and c^2 has been inserted to convert from geometric to international system units. The same cup placed on the opposite side of the clump at $r + R$ would undergo the force $F_{\rm eff} = \mu' c^2 (\frac{dV_{\rm eff}}{dr})_{r+R}$; therefore, the tidal force over the clump of matter is (see also Ref. [59])

$$F_T = \mu' c^2 \left[\left(\frac{dV_{\rm eff}}{dr}\right)_{(r-R)} - \left(\frac{dV_{\rm eff}}{dr}\right)_{(r+R)}\right] \approx \mu' c^2 2R \left(\frac{d^2 V_{\rm eff}}{dr^2}\right)_r \quad (5)$$

where $\approx$ indicates that we used a Taylor sum in R/r up to the first order since we expect $R \ll r$. The tidal force cannot be larger than the ultimate tensile strength σ of the material[3] (times the area $2\pi Rh$ of the cup), i.e., $F_T \leq 2\pi Rh\sigma$. From this inequality we can get some order of magnitude on the maximum radius R allowed by tides

$$R = \left(10\left(1 - \frac{1}{30}\right)^{-1} \frac{c_s^2}{c^2}\frac{\sigma}{Y} \times \left(-\frac{2m}{r^3} + \frac{3\tilde{L}^2}{r^4} - \frac{12m\tilde{L}^2}{r^5}\right)^{-1}\right)^{1/2} \quad (6)$$

where we write the density $\rho = Y/c_s^2$, Y is the Young's modulus of the material, and c_s the speed of sound in it. In the case of a solid-state material, e.g., asteroids,[4] iron/steel-like material has a typical ratio in the laboratory $\sigma/Y \sim 5 \times 10^{-3}$ ($\sigma \sim 10^2$ MPa, $Y \sim 10^2$ GPa [60]) and $c_s = 5 \times 10^5$ cm/s. From (6) the upper limit on the radius R of a solid-state clump that can survive to tides, at a distance $r \sim 6 - 10 r_g$ from a $2M_\odot$ neutron star, is $\sim$30 cm (see also Ref. [61]). The rest-mass energy of a such sphere made of iron or steel ($\rho \sim 8$ g/cm^3) is $\mu c^2 \sim 10^{27}$ erg; thus, from Fig. 2 only $\sim 6 \times 10^{23}$ erg can be emitted at the maximum of the bell-shaped curve. This is too low for the observed energy of the lower HFQPO whose amplitude is some percent of the luminosity of the source, i.e., $10^{34} - 10^{36}$ erg/s. Hence, solid-state clumps made of iron/steel-like material (e.g., asteroids) are disfavored as sources of the lower HFQPO.

IV. SIZE ALLOWED BY THE STRONG TIDES OF ORBITING CLUMPS OF MATTER: THE PLASMA CASE

The plasma material in the accretion disk has different mechanical properties than solid-state matter. However, it may raise some doubts thinking that clumps of plasma in the accretion disk can survive to the strong shear forces due to differential rotation and are thus not able to produce the lower HFQPO. On the other hand, to our knowledge, detailed simulations showing that clumps of plasma cannot produce QPOs in the power spectra are not reported in the literature. Instead, there is a numerical code [52] showing that orbiting clumps around a compact object can produce power spectra with twin-peak QPOs [53]. In this numerical code the clump is a collection of free particles. Each particle has its own geodesic. By means of ray-tracing techniques in the Schwarzschild metric, the code shows that the signal from the clump, disrupted by both shear forces and tides, can produce twin QPOs. Most recently, Germanà [62] argued that the timing law of the azimuth phase $\phi(t)$ on elliptical relativistic orbits could be the root for the appearance of multiple peaks in the power spectrum. Bakala *et al.* [5] modeled in detail the signal produced by orbiting hot spots. Although the issue of a lower HFQPO produced by orbiting clumps in the disk may be an open debate, it is a viable interpretation. We should bear in mind that the observed central frequency of the lower HFQPO is typical of the orbiting matter close to the compact object [2–5,21]. Moreover, the numerical code in Ref. [52] shows that *already* clumps of free particles can produce a lower HFQPO [53]. In reality, since the clumps of plasma in the disk might have some internal force, it is even more probable that they produce the lower HFQPO. Thus, it might be worthwhile to investigate the mechanical properties of clumps of plasma in the accretion disk.

We estimate the density of the inner part of the accretion disk by using the equation of the density of the disk reported in Ref. [57]. For typical accretion rates in NS LMXBs of $\sim 10^{18}$ g/s [Eq. (1.7) in Ref. [57]; a Z source with luminosity $L = L_{\rm Edd} \sim 2.5 \times 10^{38}$ erg/s [40], where $L_{\rm Edd}$ is the Eddington limit], for a $2M_\odot$ neutron star and at a distance of $r \sim 6 - 10 r_g$, the density of the material in the

[3] In our Solar System there are moons orbiting the parent planet below their gravitational Roche radius. They are held together by electrochemical bonds stronger than their self-gravity. Metis and Pan are moons orbiting below their gravitational Roche radius.

[4] Even if an asteroid would probably be vaporized by the strong x-ray field ($T \sim 10^7$ K) far away the compact object, we consider this case for the sake of completeness.

disk is ~ 10 g/cm^3, like that of iron. Because it is expected to be a highly ionized plasma, the speed of sound c_s is not like that in iron materials. We write [57]

$$c_s = \left(\frac{\gamma Z k T}{m_i}\right)^{1/2} \tag{7}$$

where $\gamma \sim 5/3$ is the adiabatic index, Z the charge state ($Z = 1$ for a hot plasma), m_i the ion hydrogen mass, and k the Boltzmann's constant. For typical temperatures in the inner part of the accretion disk of $T \sim 4 \times 10^7$ K, it turns $c_s \sim 8 \times 10^7$ cm/s.

From (6) the upper limit by tides on the size of the clump depends also on the ratio σ/Y. This quantity describes the malleability of the body to external deformations, or, following the Hooke's law ($\sigma = Y\epsilon$), it tells us how much deformable the material is before breaking. In the following, we explore the idea of characterizing clumps of plasma through the ratio σ/Y. This way of proceeding might be justified by the results reported by Corral-Santana *et al.* [63] who discovered large structures in the accretion disk of an x-ray binary system. Such structures propagate through the disk. Thus, it is hard to think to a completely smoothed accretion disk, but rather it might be characterized by inhomogeneities propagating throughout it. If inhomogeneities of plasma exist, as reported in Ref. [63], they have to be held together by some internal force (e.g., Ref. [64]) against tides and differential rotation. Whatever the nature of this force is, its value per unit area displays an ultimate tensile strength of the material. Equivalently, such force can be characterized through the mechanical binding energy, defined as the energy required to disaggregate/separate a body [65]. The binding energy per unit volume is the ultimate tensile strength σ [66].

In this context, it might be worth noting that some features of the accretion disk theory are still open to debate. King *et al.* [67,68] pointed out the yet unclear understanding about the viscosity in accretion disk models. They investigated the disagreements between the viscosity parameter α required from observations and the one from simulations. King *et al.* [67] remark that α is not unambiguously the viscosity in the Navier-Stokes equation but rather we can think of it as the ratio of the stress to the rate of strain of the plasma. Its real physical meaning remains unclear.

A. Constrain the ratio σ/Y of clumps of plasma in the accretion disk

We estimate the ratio σ/Y recalling the binding energy of a body. The gravitational binding energy of a uniform sphere of mass M and radius R is defined as the energy required to separate it in small parts and bring them at an infinite distance. The formula reads $E_b = 3GM^2/5R$ [65]. This is valid for a body of loose material held together by only gravity. We are dealing with clumps of hot-dense plasma, held together by some internal force. If σ is the ultimate tensile strength to be applied to break a specimen of such material, i.e., an energy per unit volume [66], the energy required to disaggregate a body of volume V is the mechanical binding energy

$$E_b = \sigma V = \frac{4}{3}\pi R^3 \sigma. \tag{8}$$

Substituting R from (6) we obtain

$$\frac{\sigma}{Y} = \left(\frac{3}{4\pi}\left(\frac{1}{10}\right)^{3/2}\left(1-\frac{1}{30}\right)^{3/2}\frac{E_b}{Y}\left(\frac{c}{c_s}\right)^3 \times \left(-\frac{2m}{r^3}+\frac{3\tilde{L}^2}{r^4}-\frac{12m\tilde{L}^2}{r^5}\right)^{3/2}\right)^{2/5}. \tag{9}$$

Accreting clumps of plasma once disrupted by tides should release an energy that is at least of the same order of E_b. Thus, such binding energy may be of the order of that emitted by the lower HFQPO. For a Z source, the amplitude of the lower HFQPO is $\sim 2\% - 4\%$ the luminosity of the source [40]. We shall write $E_b \sim 5 \times 10^{36}$ erg. Knowing the Young's modulus $Y = \rho c_s^2$ for the clump of plasma, we get $\sigma/Y \sim 70$. A ratio $\sigma/Y > 1$ means a deformation after breaking as big as more than once the initial size of the body. This is the case for, e.g., an elastic rope. Thus, a $\sigma/Y \sim 70$ means that the clump of plasma is far more deformable than solid-state iron materials. Because of this higher malleability to external deformations, (6) gives a bigger upper limit on the size of the structure of plasma that sustains tides, $R \sim 6500$ m.

In Sec. IV we mentioned that already clumps of free particles orbiting a compact object can produce the lower HFQPO [53]. Here the clump of plasma is held together by an internal force characterized by σ. We calculate whether the large upper limit of $R \sim 6500$ m set by tides can sustain the strong shear forces due to differential rotation. We divide the structure into, say, 10 slices and calculate the differential velocity as

$$dv = 2\pi r\left(\frac{GM}{4\pi^2 r^3}\right)^{1/2} - 2\pi r'\left(\frac{GM}{4\pi^2 r'^3}\right)^{1/2} \tag{10}$$

where r is the radius of the orbit at the center of the clump, and $r' = r + dh$ is the orbital radius of a contiguous slice. The shear force between two contiguous slices is

$$F = \rho \nu_k dV dv \tag{11}$$

where $\rho \sim 10$ g/cm^3 is the density of the plasma, $dV = 2\pi R^2 dh$ is the volume of the slice, and ν_k the Keplerian frequency. It turns out that such a load is $F = 10^{24}$ N. The ultimate tensile strength $\sigma \sim 70Y$ gives an opposite force keeping the slices together at $2\pi R^2 \sigma \sim 10^{25}$ N.

V. ENERGY LOADED BY TIDES ON ORBITING CLUMPS OF PLASMA

With the limits on the size of the clump of plasma estimated above, we may now give constrains on both the energy that tides might deposit on the orbiting clump and the amount of removed orbital energy (3) per periastron passage. This will give us information on the interval of orbits the clump spirals over before disrupting and constrain how much potential energy is released, to compare it to the observations.

The rate of energy deposited by tides on the orbiting clump of plasma is [69]

$$\frac{dE}{dt} = \int dx^3 \rho \mathbf{v} \cdot \boldsymbol{\nabla} V_{\text{eff}} \tag{12}$$

where $\mathbf{v}$ is the velocity of an element of the clump because of the perturbation by tides. We shall write $|\mathbf{v}| = dR/dt$, with R radius of the clump. We turn the integral in time into an integral over the orbit, multiplying by dt/dr

$$\frac{dE}{dr} = \int dx^3 \rho \frac{dR}{dr} \nabla V_{\text{eff}}. \tag{13}$$

The term dR/dr simulates the deformation of the clump because of tides as a function of the distance r from the central object. On a slightly eccentric orbit dR/dr oscillates because of the changing tidal force between periastron and apastron. At $r \sim 8r_g$ the tidal force (5) per unit area over a clump of plasma $R = 3200$ m is $\sigma_T \sim 10^{17}$ Pa, while the ultimate tensile strength of the material $\sigma = 70Y \sim 5 \times 10^{17}$ Pa. Thus, the clump may undergo some elastic phase before breaking.[5] The tidal stress σ_T slightly oscillates (by a factor $\sim$2) from periastron to apastron on a time scale[6] $t = 1/\nu_r \sim 3 \times 10^{-3}$ s.

Because $\sigma_T < \sigma$, to get order of magnitudes we treat the clump as a simple elastic body deformed by tides. We make use of the Hooke's law $d\sigma = YdR/R$; i.e., an infinitesimal variation of the load causes an infinitesimal relative deformation proportional to the Young's modulus Y of the material. The term dR/dr in (13) turns into $(R/Y)d\sigma/dr$ and since the load σ is the tidal force (5) per unit area

$$\frac{dE}{dr} = \frac{1}{4\pi RY} \int dx^3 \rho \frac{dF_T}{dr} \nabla V_{\text{eff}}. \tag{14}$$

[5]Structures equal/larger than the limits constrained in Sec. IV A cannot survive at all because of tides. On the other hand, structures smaller than $R \sim 3000$ m would not be able to emit the required energy seen in the lower HFQPO in Z sources, i.e., $\sim 5 \times 10^{36}$ erg/s.

[6]ν_r is the relativistic radial frequency of the orbit. In the Schwarzschild metric around a $2M_\odot$ neutron star $\nu_r \sim 350$ Hz at its maximum ($r \sim 8r_g$).

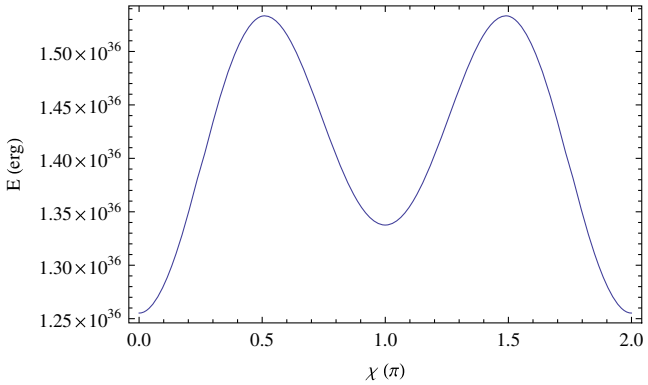

FIG. 3 (color online). Energy loaded by tides on a clump of plasma of radius $R = 3200$ m as a function of the radial phase χ of the orbit.

The tidal force is constant over the clump at a given r. The integral over the volume, after transforming it in spherical coordinates, reads $\approx 4\pi R^3 (dV_{\text{eff}}/dr)_r$ in the approximation $R \ll r$. Substituting (5) into (14) and integrating over the radius of the orbit, we obtain an estimate on the energy loaded by tides on the clump

$$\begin{aligned} E(r) = {} & \frac{3\pi\rho c^4 R^6}{6.6 \times 10^3 c_s^2 r^9} \\ & \times (20\tilde{L}^4(21mr - 35m^2 - 3r^2) - 42m^2 r^4 \\ & -15\tilde{L}^2 mr^2(26m - 7r)). \end{aligned} \tag{15}$$

We insert into (15) the parametrized radius [54]

$$r(\chi) = \frac{pm}{1 + e\cos(\chi)}. \tag{16}$$

Figure 3 shows the behavior of the energy loaded by tides[7] (15) on the clump of plasma as a function of the radial phase χ. The curve is symmetric with respect to the apastron at $\chi = \pi$. The orbit has the periastron at $8r_g$ and eccentricity $e = 0.1$, around a $2M_\odot$ neutron star.[8]

Such energy is transferred from orbit to internal energy through tides [58,69]. A removal of orbital energy of $\sim 10^{36}$ erg from (3) gives a spiral motion of $0.4r_g \sim 1200$ m after the first periastron passage on these orbits with low $e = 0.1$. The tidal wave propagates through the clump on a time scale $\tau = 2R/c_s$. The radius of the fraction of the clump disrupted between two periastron passages is $R_l = tc_s/2 \sim 1100$ m. On the second periastron passage the radius of the clump might be smaller ($R \sim 2000$ m); the energy deposited by tides (15) now is $E(r) \sim 10^{35}$ erg

[7]Note that the order of magnitude estimated here $E(r) \sim 0.12\%\ \mu c^2$ agrees with that from the formalism described in Ref. [46] for a star disrupted by a supermassive black hole.

[8]All over the window of periastra $\sim 5.6 - 10r_g$ the energy deposited on the clump $R = 3200$ m is $\sim 10^{36}$ erg.

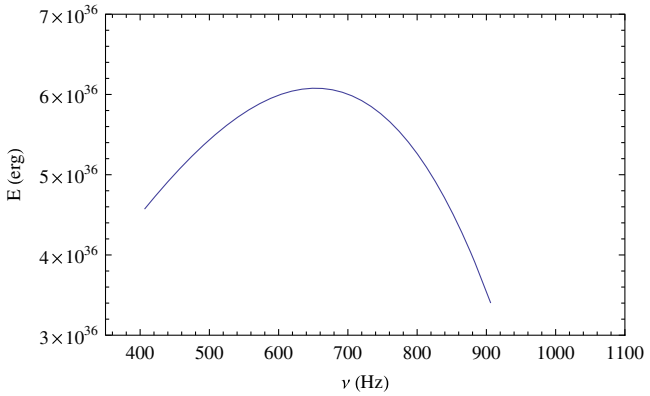

FIG. 4 (color online). Difference of potential energy at periastron between two orbits with periastra ∼1700 m away as a function of the orbital frequency. To compare it to the data see Fig. 1 in Ref. [42], Fig. 3 in Ref. [38], and Fig. 2 in Ref. [40].

causing a spiral motion of $0.1r_g \sim 300$ m. On the third periastron passage, what is left has a radius $R \sim 1000$ m $< R_l$. The energy deposited by tides on such a relic at each periastron passage is $E(r) \sim 10^{33}$ erg, causing a spiral motion of $0.01r_g \sim 30$ m. The binding energy (8) is $E_b \sim 10^{34}$ erg. Thus, the number of periastron passages before disrupting may be ∼10. In total the clump might make ∼12 periastron passages. The number of Keplerian turns is[9] ∼24. The difference of potential energy between the orbits is emitted by such an event on a time scale $\tau' = 12/(350\ \text{Hz}) \sim 0.034$ s. The coherence as defined in Sec. I $Q = \nu/\Delta\nu$ in this case is $Q = \nu_k\tau' \sim 24$, corresponding to the number of Keplerian turns.

In total, the initial clump with $R = 3200$ m has spiraled over an interval of orbits $\sim 0.6r_g \sim 1700$ m. Figure 4 shows the differences of potential energy, at periastron, released between two orbits with periastra ∼1700 m away as a function of the orbital frequency[10] around a $2M_\odot$ Schwarzschild compact object (the curve spans over $r \sim 10 - 6r_g$). It displays the characteristic bell shape centered at $\sim 700 - 800$ Hz[11] seen in the observations [38–40,42]. The emitted energy matches that carried by the lower HFQPO in Z sources [40] and corresponds to $\sim 0.5\%\ \mu c^2$. The figure corresponds to the maximum of the overall bell shape in Fig. 2. Because the bell shape in Fig. 4 is typical of the observed amplitude behavior of the lower HFQPO rather than the upper one, this study may add one more clue: it suggests that the lower peak of the observed twin peaks corresponds to the Keplerian frequency. This is in agreement with the results from the numerical code on tidal disruption [53], where the lower HFQPO corresponds to the Keplerian modulation ν_k while the upper HFQPO to the modulation at $\nu_k + \nu_r$. Such a conclusion is also reported in Ref. [62]. Models proposing other mechanisms to produce HFQPOs and assuming the lower HFQPO to be ν_k have been previously proposed [18–20], differently than in Refs. [2,3,16,17] in which the upper HFQPO is linked to ν_k.

The lower HFQPO is observed to range $\sim 600 - 950$ Hz [38–40,42]. From Fig. 4 we deduce that the clustering might be because the difference of potential energy released by such random events between near orbits has its maximum in the region of the space-time $r \sim 10 - 6r_g$ (see also Fig. 2). The steeper decrease in Fig. 4 is drawn by the approach to ISBO (see also Fig. 2). Hence, the observed behavior of the amplitude of the lower HFQPO as a function of its central frequency may give clues related to the ISBO predicted by GR in a strong field regime ($r \sim r_g$).

VI. THE KERR METRIC CASE

We performed our calculations in the case of a rotating compact object, whose space-time around it is described by the Kerr metric [70]. The effective radial gravitational potential $V_{\text{eff,Kerr}}$ is such [13] that for a nonrotating compact object ($a = 0$, a is the angular momentum per unit mass of the compact object) we get (1)

$$V_{\text{eff,Kerr}} = 1 - \frac{2m}{r} + \frac{a^2}{r^2} + \left(1 + \frac{2m}{r}\right)\frac{a^2\tilde{E}_{\text{orb}}^2}{r^2} + \frac{4am\tilde{E}_{\text{orb}}\tilde{L}}{r^3} + \left(1 - \frac{2m}{r}\right)\frac{\tilde{L}^2}{r^2} \tag{17}$$

with $0 \le a \le m$, $\tilde{E}_{\text{orb}}$, and $\tilde{L}$ orbital energy and specific angular momentum of the orbiting particle, respectively, on a generic circular orbit in the Kerr metric [13].

We note that the Kerr parameter a lowers the maximum radius R of the clump of plasma allowed by tides: for an orbit at $8r_g$ $R \sim 7000$ m[12] for $a = 0$, and $R \sim 6500$ m for $a = 0.9m$. The work done by tides per periastron passage remains of the same order of that obtained in the Schwarzschild metric [Eq. (15), $E(r) \sim 10^{36}$ erg]. Thus, the clump with size $R = 3200$ m as in Sec. V makes an almost equal number of turns before disrupting, spiraling over an interval of orbits of $\sim 0.6r_g \sim 1700$ m. Figure 5 shows the difference of Kerr potential energy released for different values of a between orbits ∼1700 m away. We see

[9]Around the region $r \sim 8r_g$ the ratio of the relativistic Keplerian frequency ν_k to the radial one ν_r is $\nu_k/\nu_r \sim 2$. Thus, if the number of periastron passages is n, the number of Keplerian turns is $2n$.

[10]We calculated the orbital frequency for an orbit with $e = 0.1$ by means of the integrals reported in Ref. [54] describing both the azimuth phase $\phi(\chi)$ and coordinate time $t(\chi)$ in the Schwarzschild metric, for generic orbits of eccentricity e. We resolved them by applying a Taylor sum around $e = 0$ [62].

[11]For a $1.8M_\odot$ compact object, the curve in Fig. 4 is centered around 800 Hz.

[12]This value agrees to that from (6) for an orbit with $e = 0$.

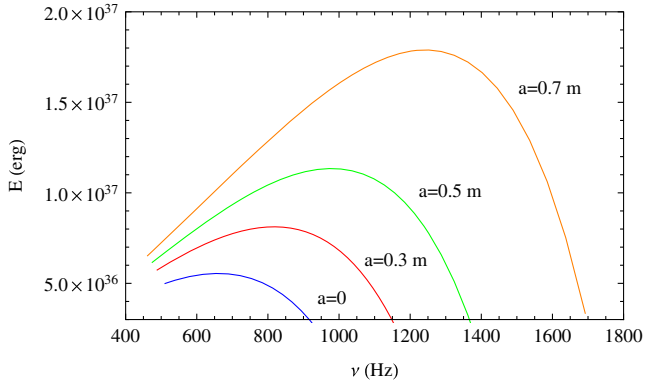

FIG. 5 (color online). Differences of Kerr/Schwarzschild potential energy expected to be released by an orbiting clump of plasma of radius $R = 3200$ m after being disrupted by tides. The curves refer to different values of the Kerr parameter a.

that such a mechanism is more efficient for increasing a: the amplitude of the bell-shaped curve increases. The effect of a is also to move the ISBO to the inner regions, so that the orbital frequency extends to higher values. The figure refers to a $2M_\odot$ compact object. For a $2.5M_\odot$ each curve in the figure is almost shifted to lower frequencies by ∼200 Hz. It is known that different couples (m, a) could describe the same frequency at a given orbital radius [32]. Instead the value of the mass has no effects on the amplitude of the bell-shaped curves in Fig. 5.

VII. OTHER FACTORS AFFECTING THE AMPLITUDE OF THE LOWER HFQPO

We advise caution about the behavior shown in Figs. 4 and 5 and seen in the observations [38–40,42] as a candidate to disclose a signature of ISBO. We discuss below other factors that may affect the amplitude of the lower HFQPO.

A. The dependence of the amplitude on the energy

The amplitude of the lower HFQPO measured at different energy channels keeps increasing towards hard x ray. At $\sim 20 - 30$ keV the amplitude of the lower HFQPOs is ∼20%, while at ∼2 keV it is less than 5% [42,71]. The lower HFQPO is usually stronger in the hard state of the source, where the energy spectrum is dominated by a power law. This means that the thermal emission from a Keplerian disk cannot justify its nature. A corona of hot electrons scattering the seed photons from the disk to higher energy has been proposed [72–75]. On the other hand, Schnittman [76] noted that this mechanism may not amplify the modulation, but rather would lower the amplitude of the modulation at high energies, since the scattering of photons by hot electron would smooth the oscillation from the disk.

Alternatively to the corona scenario, the modeling in Ref. [77] shows that sub-Keplerian motion in the inner part of the accretion disk ($r \lesssim 20 r_g$) might cause a postshock region with hard x-ray emission. Hard x-ray emission also might come from the converging bulk motion of the accreting matter. In Ref. [78] it is shown that in such a sub-Keplerian region the specific angular momentum of the accretion flow can also behave in a Keplerian way. Therefore, Keplerian imprints like that described in our manuscript may be seen in the observed hard state.

Yan and Wang [79] pointed out the idea that the hard x-ray spectrum of the lower HFQPO might originate by synchrotron mechanisms from a magnetized hot spot. Calculations on the radiation that would be emitted by a tidally disrupted magnetized clump of matter were attempted in Refs. [52,80] and full magnetohydrodynamic simulations are demanded. Thus, the exact energy emission mechanism of the lower HFQPO may remain of open debate and is far beyond the goal of this paper. This manuscript attempts to propose a mechanism justifying how the quantity of energy carried by the lower HFQPO would originate and not the energy spectrum of the emission, which depends on the exact nature of the energy emission mechanism. We are comparing our calculations to bolometric luminosity. Gravitational energy is extracted through tides and transformed into radiation through a given emission mechanism. The bolometric luminosity emitted should be equal to the amount of gravitational energy extracted. Thus, the behavior in Figs. 4 and 5 and seen in the observations [38–40,42] may still remain a candidate to disclose a signature of ISBO.

B. The dependence of the amplitude on the luminosity of the source

It is known that the amplitude of the lower HFQPO is different among sources with different luminosity, i.e., accretion rate. The amplitude of the lower HFQPO is up to ∼20% in atoll sources, while in Z sources it is ∼5%. Z sources have a luminosity (∼10^{38} erg/s) that can be up to 2 orders of magnitude higher than atoll (∼10^{36} erg/s) [40]. The unique source XTE J1701-462 displays both phases, i.e., atoll and Z [81]. In Fig. 4 of Ref. [81] is shown the amplitude (in percent of the total luminosity of the source) in the atoll and Z phases. The same source displays different amplitudes of the lower HFQPO (10% in the atoll phase, 3% in the Z phase) at the same central frequency of the peak. Thus, it has been suggested that the amplitude of the lower HFQPO as a function of its central frequency within a source (e.g., Figs. 4 and 5 in this paper, Fig. 1 in Ref. [42], Fig. 3 in Ref. [38], and Fig. 2 in Ref. [40]) may not be simply used as clue related to a signature of ISBO [81]. The study proposed in this manuscript may offer a possible interpretation to these differences between atoll and Z sources.

In the Z phase XTE J1701-462 has a luminosity of $L \sim 0.5 L_{\rm Edd} \sim 10^{38}$ erg/s (Fig. 5 in Ref. [81]), where $L_{\rm Edd} \sim 2.5 \times 10^{38}$ erg/s is the Eddington luminosity for a $\sim 2M_\odot$ neutron star [57]. The accretion rate of the source is

$\dot{M} \sim 7 \times 10^{17}$ g/s. The lower HFQPO has a coherence up to $Q \sim 30$ and amplitude ~3%, corresponding to $\sim 3 \times 10^{36}$ erg/s. At lower accretion rates ($\dot{M} \sim 7 \times 10^{16}$ g/s) in the atoll phase the coherence is up to $Q \sim 150$ and the amplitude up to ~10%, also corresponding to $\sim 2 \times 10^{36}$ erg/s (for such details see Fig. 5 in Ref. [81]). From the calculations in Sec. IV A and Sec. V we obtain that in the Z phase structures as large as $R \sim 3000$ m can survive to tides, making 10 periastron passages, producing an oscillation with coherence $Q \sim 20$ (typical of the Q observed in XTE J1701-462 in its Z phase [81]) and emitting the observed energy of the lower HFQPO $\sim 3 \times 10^{36}$ erg, corresponding to ~0.6% μc^2. The limiting size R_l given by the accretion rate is $R_l \sim 900$ m. The initial clump with $R = 3000$ m spirals over an interval of orbits of $0.73 r_g \sim 2100$ m.

In the atoll phase of XTE J1701-462 the accretion rate is $\dot{M} \sim 7 \times 10^{16}$ g/s and the lower HFQPO has also a luminosity $\sim 10^{36}$ erg/s (10% of the luminosity of the source). Because of the lower accretion rate, the density is lower by a factor ~5 ($\rho \sim 1\ g/\mathrm{cm}^3$) than in the Z phase. A structure with $R \sim 3000$ m can spiral over $1.5 r_g$ and emits $\sim 2 \times 10^{36}$ erg, corresponding to 1.3% μc^2. The limiting size is $R_l \sim 500$ m and this last stage lasts for ~60 periastron passages, spiraling over $0.2 r_g$. Thus, the lower HFQPO has a coherence of $Q \sim 130$, much higher than that in the Z phase, as in the observations [81].

We did the calculations also for the source 4U 0614 + 09, which has the lowest luminosity in Fig. 5 in Ref. [81] (see also Fig. 3 in Ref. [40]). Its accretion rate is $\dot{M} \sim 7 \times 10^{15}$ g/s and the maximum luminosity of the lower HFQPO is $\sim 10^{35}$ erg/s (~10% that of the source). The limiting size given by the typical speed of sound c_s is $R_l \sim 400$ m, the density of the plasma $\rho \sim 0.5\ \mathrm{g/cm}^3$ (1 order of magnitude lower than Z sources). An initial structure with $R \sim 2500$ m spirals by $0.8 r_g$, $0.4 r_g$, $0.2 r_g$, $0.1 r_g$, and $0.03 r_g$ after the first, second, etc. periastron passage. Afterwards the relic reaches the limiting size $R \sim R_l$ and spirals by $0.003 r_g$ per periastron passage, making ~15 passages. In total, it might make ~20 periastron passages before disrupting ($Q \sim 40$). The energy emitted is $\sim 3 \times 10^{35}$ erg corresponding to ~1.2% μc^2.

In Z sources the clump makes a similar number of turns before disrupting. The allowed number of turns by tides might be dictated by the bigger size R_l, allowing tides to make more work per periastron passage.

Figure 6 shows the simulated coherence Q of the Keplerian oscillation obtained with such a mechanism for both the atoll and Z phases of XTE J1701-462 and the lowest luminosity source 4U 0614 + 09. The figure reproduces the observed coherence of the lower HFQPO as a function of the luminosity (accretion rate) of the source (Fig. 5 in Ref. [81] and Fig. 3 in Ref. [40]). These results suggest that the lower HFQPO might correspond to the Keplerian modulation of orbiting matter around the compact object, similar to what the results in Sec. V suggest.

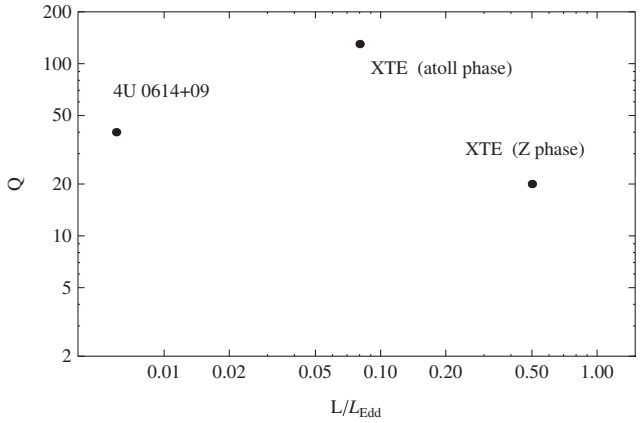

FIG. 6. Simulated quality factor Q (coherence) of the Keplerian modulation by an orbiting clump of plasma as a function of the luminosity L of the source (in units of the Eddington luminosity $L_{\mathrm{Edd}} \sim 2.5 \times 10^{38}$ erg/s) for two representative sources (see text). Such coherences are typical of the lower HFQPO in these sources (see Fig. 5 in Ref. [81] and Fig. 3 in Ref. [40] for a comparison with the data).

From the mechanism proposed here, we see that structures of plasma with size $R \sim 3 \times 10^3$ m (at an orbital radius $r \sim 8 r_g \sim 24$ km, $R/r \sim 0.1$) are required to produce the observed luminosity of the lower HFQPO among a sample of sources with different accretion rates. They would emit an energy that is $\sim 10^{36}$ erg in both atoll and Z sources (~10% and ~3% the total luminosity, respectively) and in the lowest luminosity state (e.g., 4U 0614 + 09 with density of the plasma 1 order of magnitude lower) $\sim 10^{35}$ erg. They might produce Keplerian modulations with different coherences similar to the observations (Fig. 6), because of the interplay between tides and the mechanical properties of the plasma.

Speaking about orders of magnitude, we notice that the size of the structure required to emit the observed energy is similar among a sample of sources spanning ~2 orders of magnitude in luminosity. The geometry of the space-time because of the neutron star might play a relevant role among the sample of sources. Larger structures may not survive/form at all because of tides. This may justify why we do not observe an amplitude of the lower HFQPO of, e.g., 10%–20% in Z sources ($\sim 10^{37}$ erg/s), or higher than those observed in atoll sources. From (9) we derive $\sigma/Y \sim 70$ in the Z state of XTE J1701-462 and also for the Z source in Sec. IV A. $\sigma/Y \sim 300$ in the atoll states, i.e., both the atoll phase of XTE J1701-462 and 4U 0614 + 09, even if they differ by 1 order of magnitude in luminosity. Thus, the atoll and Z states of LMXBs may characterize some properties of the plasma in the accretion disk (e.g., electrochemical bonds and/or magnetohydrodynamical).

To conclude, different accretion flows between Z and atoll sources might change the mechanical properties of the

clumps of plasma, such as ρ, c_s, Y, and σ/Y, in a way that both the amplitudes and coherences of the lower HFQPO also depend on the accretion flow [81]. However, within a source that does not change dramatically its accretion rate, the behavior of the amplitude of the lower HFQPO with its central frequency (i.e., Figs. 4 and 5 in this paper, Fig. 1 in Ref. [42], Fig. 3 in Ref. [38], and Fig. 2 in Ref. [40]), after this analysis, may still remain a candidate for a signature of ISBO.

VIII. REMARKS AND CONCLUSIONS

Reis *et al.* [49] reported a QPO in the x-ray flux from the tidal disruption of a star by a supermassive black hole. Here we have shown that the amplitude of the lower HFQPO in NS LMXBs might display the Schwarzschild/Kerr potential energy released by spiraling clumps of plasma in the accretion disk. By means of first-approximation calculations, this mechanism gives orders of magnitude typical of the observed energy carried by the lower HFQPO. We would stress that magnetohydrodynamic modeling is certainly required to reach firmer conclusions. The estimations reported here are promising and are shown for the first time.

The mechanical properties of the plasma (c_s, Y, σ/Y) in the accretion disk depend on its density and temperature and, therefore, on the accretion rate of the source. This study suggests that both the amplitude and coherence of the lower HFQPO also might depend on the interplay between the mechanical properties of the clumps (c_s, Y, σ/Y) and the work done by tides on them. Such differences among sources with different accretion rates are reported in Ref. [40,81] and were also discussed in Ref. [41].

The main and new results of this study are (i) the differences of Schwarzschild/Kerr potential energy emitted by spiraling clumps of plasma might account for the observed energy (amplitude) carried by the lower HFQPO. Also, the coherence time obtained from the time scale of tidal disruption ($\sim 0.03 - 0.2$ s) is typical of the observed ones ($\sim 0.01 - 0.2$ s; Refs. [38–40,81]). This is the first time that a proposed physical mechanism can justify both the observed emitted energy and coherence of the lower HFQPO. We are able to give an interpretation to the different coherence of the lower HFQPO among a sample of sources with different luminosity (Fig. 6). (ii) Within a source with a given accretion rate, the typical bell shape of the amplitude of the lower HFQPO as a function of its central frequency (seen in the data collected from several NS LMXBs [38–40,42]) might be reproduced by differences of Schwarzschild/Kerr potential energy between near orbits over the region $r \sim 6 - 10 r_g$. Thus, such bell-shaped behavior may be related to the terms $\propto 1/r^3$ in (1) and (17) in a strong field regime and therefore could be a geometry-related effect due to ISBO (Figs. 2, 4, and 5). We, however, would stress that the Schwarzschild and Kerr metrics only approximate the space-time around a neutron star [78]. (iii) Our calculations might justify for the first time the interval of radius where the lower HFQPO is produced, i.e., $\sim 6 - 10 r_g$: in this region the highest difference of potential energy is released between the orbits the clumps spiral over before disrupting (Fig. 2). Future observations with a higher signal to noise ratio [82] could extend this region which, with the data to date, may just be masked by the background radiation from the disk.

ACKNOWLEDGMENTS

We thank the anonymous referee for constructive criticism that improved this manuscript. C. G. thanks the program PNPD/CAPES-Brazil for full support. R. C. is grateful to CNPq, CAPES, and FAPEMA (Brazilian agencies) for their financial support. We thank Adalto Gomes, Manoel Ferreira Jr., and Rodolfo Angeloni for the stimulating discussions on the topic.

[1] M. van der Klis, J. H. Swank, W. Zhang, K. Jahoda, E. H. Morgan, W. H. G. Lewin, B. Vaughan, and J. van Paradijs, Astrophys. J. Lett. **469**, L1 (1996).
[2] M. C. Miller, F. K. Lamb, and D. Psaltis, Astrophys. J. **508**, 791 (1998).
[3] L. Stella, M. Vietri, and S. M. Morsink, Astrophys. J. Lett. **524**, L63 (1999).
[4] J. D. Schnittman and E. Bertschinger, Astrophys. J. **606**, 1098 (2004).
[5] P. Bakala, G. Török, V. Karas, M. Dovčiak, M. Wildner, D. Wzientek, E. Šrámková, M. Abramowicz, K. Goluchová, G. P. Mazur, and F. H. Vincent, Mon. Not. R. Astron. Soc. **439**, 1933 (2014).
[6] R. V. Wagoner, A. S. Silbergleit, and M. Ortega-Rodríguez, Astrophys. J. Lett. **559**, L25 (2001).
[7] C.-k. Chan, Astrophys. J. **704**, 68 (2009).
[8] R. V. Wagoner, Astrophys. J. Lett. **752**, L18 (2012).
[9] W. Kluzniak, P. Michelson, and R. V. Wagoner, Astrophys. J. **358**, 538 (1990).
[10] W. Zhang, A. P. Smale, T. E. Strohmayer, and J. H. Swank, Astrophys. J. Lett. **500**, L171 (1998).
[11] F. K. Lamb, ASP Conf. Ser. **308**, 221 (2003).
[12] M. van der Klis, arXiv:astro-ph/0410551.
[13] J. M. Bardeen, W. H. Press, and S. A. Teukolsky, Astrophys. J. **178**, 347 (1972).
[14] L. Stella and M. Vietri, Phys. Rev. Lett. **82**, 17 (1999).

[15] V. Karas, Astrophys. J. **526**, 953 (1999).
[16] S. E. Motta, T. M. Belloni, L. Stella, T. Muñoz-Darias, and R. Fender, Mon. Not. R. Astron. Soc. **437**, 2554 (2014).
[17] S. E. Motta, T. Muñoz-Darias, A. Sanna, R. Fender, T. Belloni, and L. Stella, Mon. Not. R. Astron. Soc. **439**, L65 (2014).
[18] V. Osherovich and L. Titarchuk, Astrophys. J. Lett. **522**, L113 (1999).
[19] L. Titarchuk and V. Osherovich, Astrophys. J. Lett. **518**, L95 (1999).
[20] B. Mukhopadhyay, S. Ray, J. Dey, and M. Dey, Astrophys. J. Lett. **584**, L83 (2003).
[21] M. A. Abramowicz and W. Kluźniak, Astron. Astrophys. **374**, L19 (2001).
[22] P. Rebusco, Astron. Nachr. **326**, 830 (2005).
[23] J. Horák and V. Karas, Astron. Astrophys. **451**, 377 (2006).
[24] Z. Stuchlík, A. Kotrlová, and G. Török, Astron. Astrophys. **552**, A10 (2013).
[25] J. Pétri, Astron. Astrophys. **439**, 443 (2005).
[26] W. Kluźniak, M. A. Abramowicz, S. Kato, W. H. Lee, and N. Stergioulas, Astrophys. J. Lett. **603**, L89 (2004).
[27] W. H. Lee, M. A. Abramowicz, and W. Kluźniak, Astrophys. J. Lett. **603**, L93 (2004).
[28] J. Pétri, Astron. Astrophys. **439**, L27 (2005).
[29] J. Pétri, Astron. Astrophys. **443**, 777 (2005).
[30] B. Mukhopadhyay, Astrophys. J. **694**, 387 (2009).
[31] Y.-F. Lin, M. Boutelier, D. Barret, and S.-N. Zhang, Astrophys. J. **726**, 74 (2011).
[32] G. Török, P. Bakala, E. Šrámková, Z. Stuchlík, M. Urbanec, and K. Goluchová, Astrophys. J. **760**, 138 (2012).
[33] Z. Stuchlik, A. Kotrlova, G. Torok, and K. Goluchova, Acta Astron. **64**, 45 (2014).
[34] M. G. B. de Avellar, M. Méndez, A. Sanna, and J. E. Horvath, Mon. Not. R. Astron. Soc. **433**, 3453 (2013).
[35] D. Barret, Astrophys. J. **770**, 9 (2013).
[36] P. Kaaret, S. Piraino, E. C. Ford, and A. Santangelo, Astrophys. J. Lett. **514**, L31 (1999).
[37] E. C. Ford, Astrophys. J. Lett. **519**, L73 (1999).
[38] D. Barret, J.-F. Olive, and M. C. Miller, Mon. Not. R. Astron. Soc. **370**, 1140 (2006).
[39] D. Barret, M. Bachetti, and M. C. Miller, Astrophys. J. **728**, 9 (2011).
[40] M. Méndez, Mon. Not. R. Astron. Soc. **371**, 1925 (2006).
[41] D. Barret, J.-F. Olive, and M. C. Miller, Mon. Not. R. Astron. Soc. **376**, 1139 (2007).
[42] M. Méndez, M. van der Klis, and E. C. Ford, Astrophys. J. **561**, 1016 (2001).
[43] J.-P. Luminet, L'Astronomie **99**, 429 (1985).
[44] M. J. Rees, Nature (London) **333**, 523 (1988).
[45] P. Laguna, W. A. Miller, W. H. Zurek, and M. B. Davies, Astrophys. J. Lett. **410**, L83 (1993).
[46] A. Gomboc and A. Čadež, Astrophys. J. **625**, 278 (2005).
[47] J. Guillochon, H. Manukian, and E. Ramirez-Ruiz, Astrophys. J. **783**, 23 (2014).
[48] S. Gezari *et al.*, Nature (London) **485**, 217 (2012).
[49] R. C. Reis, J. M. Miller, M. T. Reynolds, K. Gültekin, D. Maitra, A. L. King, and T. E. Strohmayer, Science **337**, 949 (2012).
[50] M. Del Santo, A. A. Nucita, G. Lodato, L. Manni, F. De Paolis, J. Farihi, G. De Cesare, and A. Segreto, Mon. Not. R. Astron. Soc. **444**, 93 (2014).
[51] E. Bozzo, A. Papitto, C. Ferrigno, and T. M. Belloni, Astron. Astrophys. **570**, L2 (2014).
[52] U. Kostić, A. Čadež, M. Calvani, and A. Gomboc, Astron. Astrophys. **496**, 307 (2009).
[53] C. Germanà, U. Kostić, A. Čadež, and M. Calvani, AIP Conf. Proc. **1126**, 367 (2009).
[54] C. Cutler, D. Kennefick, and E. Poisson, Phys. Rev. D **50**, 3816 (1994).
[55] K. Schwarzschild, Abh. Konigl. Preuss. Akad. Wissenschaften Jahre 1906, 92, Berlin, 1907 **1916**, 189 (1916).
[56] C. W. Misner, K. S. Thorne, and J. A. Wheeler, *Gravitation* (W. H. Freeman & Company, San Francisco, 1973).
[57] J. Frank, A. King, and D. J. Raine, *Accretion Power in Astrophysics* (Cambridge Univesity Press, Cambridge 2002).
[58] A. Čadež, M. Calvani, and U. Kostić, Astron. Astrophys. **487**, 527 (2008).
[59] E. Asphaug and W. Benz, Icarus **121**, 225 (1996).
[60] S. Kalpakjian and S. Schmid, *Manufacturing Processes for Engineering Materials* (Prentice Hall, Englewood Cliffs, NJ, 2007).
[61] S. S. Kokarev, Nuovo Cimento Soc. Ital. Fis. B **124**, 155 (2009).
[62] C. Germanà, Mon. Not. R. Astron. Soc. **430**, L1 (2013).
[63] J. M. Corral-Santana, J. Casares, T. Muñoz-Darias, P. Rodríguez-Gil, T. Shahbaz, M. A. P. Torres, C. Zurita, and A. A. Tyndall, Science **339**, 1048 (2013).
[64] S. Horn and W. Kundt, Astrophys. Space Sci. **158**, 205 (1989).
[65] S. Chandrasekhar, *An Introduction to the Study of Stellar Structure* (Dover Publicationm New York, 1939).
[66] E. Asphaug, E. V. Ryan, and M. T. Zuber, Asteroids III **1**, 463 (2002).
[67] A. R. King, J. E. Pringle, and M. Livio, Mon. Not. R. Astron. Soc. **376**, 1740 (2007).
[68] A. R. King, M. Livio, S. H. Lubow, and J. E. Pringle, Mon. Not. R. Astron. Soc. **431**, 2655 (2013).
[69] W. H. Press and S. A. Teukolsky, Astrophys. J. **213**, 183 (1977).
[70] R. P. Kerr, Phys. Rev. Lett. **11**, 237 (1963).
[71] M. Berger, M. van der Klis, J. van Paradijs, W. H. G. Lewin, F. Lamb, B. Vaughan, E. Kuulkers, T. Augusteijn, W. Zhang, F. E. Marshall, J. H. Swank, I. Lapidus, J. C. Lochner, and T. E. Strohmayer, Astrophys. J. Lett. **469**, L13 (1996).
[72] T. Di Salvo, L. Stella, N. R. Robba, M. van der Klis, L. Burderi, G. L. Israel, J. Homan, S. Campana, F. Frontera, and A. N. Parmar, Astrophys. J. Lett. **544**, L119 (2000).
[73] H. C. Lee, R. Misra, and R. E. Taam, Astrophys. J. Lett. **549**, L229 (2001).
[74] T. Di Salvo, N. R. Robba, R. Iaria, L. Stella, L. Burderi, and G. L. Israel, Astrophys. J. **554**, 49 (2001).
[75] A. Sanna, B. Hiemstra, M. Méndez, D. Altamirano, T. Belloni, and M. Linares, Mon. Not. R. Astron. Soc. **432**, 1144 (2013).
[76] J. D. Schnittman, arXiv:astro-ph/0502048.

[77] S. Chakrabarti and L. G. Titarchuk, Astrophys. J. **455**, 623 (1995).
[78] B. Mukhopadhyay and S. Ghosh, Mon. Not. R. Astron. Soc. **342**, 274 (2003).
[79] L.-H. Yan and J.-C. Wang, Res. Astron. Astrophys. **11**, 631 (2011).
[80] A. Čadež, U. Kostić, and M. Calvani, AIP Conf. Proc. **1205**, 30 (2010).
[81] A. Sanna, M. Méndez, D. Altamirano, J. Homan, P. Casella, T. Belloni, D. Lin, M. van der Klis, and R. Wijnands, Mon. Not. R. Astron. Soc. **408**, 622 (2010).
[82] M. Feroci *et al.*, Exp. Astron. **34**, 415 (2012).